Irza Sukmana
Mechanical Engineering Department, Engineering Faculty, Universitas Lampung, Jl. Prof. Sumantri Brojonegoro No. 1, Bandar Lampung 35145 Indonesia

Fauzi Ibrahim
Mechanical Engineering Department, Engineering Faculty, Universitas Malahayati, Jl. Pramuka No. 27, Bandar Lampung 35152 Indonesia

Mohammad Badaruddin
Mechanical Engineering Department, Engineering Faculty, Universitas Lampung, Jl. Prof. Sumantri Brojonegoro No. 1, Bandar Lampung 35145 Indonesia

Hadi Nur
Center of Advanced Materials for Renewable Energy (CAMRY), Universitas Negeri Malang, Malang 65145 Indonesia

Low Cycle Fatigue Properties of Extruded Magnesium AZ31B

The low cycle fatigue behavior of magnesium (Mg) AZ31B was observed at room temperature, in which its extrusion process led to differences in tensile and compressive stresses, with an increase in the grain structure and mechanical properties. The extrusion process results showed changes in the microstructure due to cyclic load-deformation at the longitudinal section with grain direction and shape. Furthermore, Mg AZ31B also showed transitional behavior from cyclic softening to hardening when the strain amplitude was increased. At a strain amplitude of 0.006 – 0.01 mm/mm, the Bauschinger phenomenon was observed. The effect factor was calculated by the yield stress and strain at compression stress.
Furthermore, precipitation or local failure of the second phase was the main factor that caused the Bauschinger phenomenon. The fatigue fracture characteristics based on deformation due to cyclic loading include precipitation, fatigue striation, dimples, micro-cracks, and beach mark fatigue. Therefore, the correlation of the total failure cycle with plastic and the elastic strain was obtained as an equation to predict the lifespan of Mg AZ31B.

Keywords: *extruded magnesium, low cycle fatigue, Bauschinger effect.*

1. INTRODUCTION

Several decades earlier, magnesium alloys were used as raw materials for automotive, aircraft, and electronics. However, now magnesium alloy has been used as a raw material for biodegradable biomaterials, especially Mg AZ31B. Cases of trauma and bone fractures often have problems with healing, especially in medical technology such as bone plates, bone screws, and dynamic compression plates with titanium, stainless steel, and platinum as raw materials. The main problem is that the main raw materials are not naturally degraded in the human body. Not degraded material will cause pain when removed from the human body. Mg AZ31B contains alloying elements such as Al 2.71%, Zn 0.69%, Mn 0.32%, Fe 0.002%, Si 0.18%, Cu 0.001%, Ni 0.001% and Ca 0.001% [1,2].

The advantages of using Mg AZ31B include low density, medium tensile strength, high corrosion resis–tance, biodegradability, and a tendency to be brittle [3]. Biodegradability can be interpreted as the implantation of biomaterials in the human body as a substitute for bone bolts, which can be degraded entirely without any aid or external factors [4,5]. Bone bolts with biodegradable properties are essential due to the total production cost and risks [6,7]. Regarding the data on hardness, tensile strength, and fatigue characteristics, studies and testing should be carried out gradually and continuously to enable the adaptation of the material to the human bone condition. Furthermore, the material will also experience tensile or cyclic loads during walking and running [8,9].

Indonesia has great potential in the development of magnesium-based materials. Magnesium raw materials are found like Indonesia and have the potential to be synthesized into magnesium for health applications so that products are not continuously imported from other countries. This material will be adapted to the needs of orthopedic materials that fulfill the requirements of biodegradation and biocompatibility and have mechanical properties like human bone. One of the properties that must be known is fatigue. Deformations in human bone tissue caused by disease or accidents can be corrected by implanting materials that aid healing [10-12]. This process should be tested in several stages of working conditions in which the implantation area will experience failure [13,14].

Furthermore, a large amount of plastic deformation is due to the inability of the material to withstand continuous loads. Therefore, the biomaterial experi–ences fatigue and then fracture [15,16]. Fatigue is a form of material failure in the structure due to dynamic loads that tend to rise and fall. This dynamic load continually occurs under yield strength for a long time [17,18]. Fatigue in the plastic state for short cycles below 104 is called low cycle fatigue. Meanwhile, it is called high cycle fatigue in elastic conditions between the value of 104 and 107.

Fatigue results that are obtained are used to see the strength of the material when a dynamic load is applied. Most studies about magnesium alloys are only focused on fatigue properties with large strain amplitudes and have not been explored using scanning electron micro–scopy. Therefore, this study will pay more attention to the test of relatively small amplitude and will observe the fracture results from the fatigue test. There are few studies regarding the behavior of low cycle fatigue properties of extruded Mg AZ31B in bone bolt

Received: May 2022, Accepted: July 2022
Correspondence to: Ir. Irza Sukmana, Ph.D.
Dept. or Mechanical Engineering, Faculty Engineering, Universitas Lampung, Bd. Lampung 35143, Indonesia
E-mail: irza.sukmana@eng.unila.ac id
doi:105937/fme2203422S

applications. Therefore, this study focused on the behavior of Mg AZ31B, which was tested for cyclic loading with a strain amplitude of 0.004 – 0.01 mm/mm and a constant strain rate of 0.00627 seconds. The results showed observation of softening and hardening behavior and fractography. Furthermore, the predicted lifespan of Mg AZ31B was obtained using the Coffin – Manson – Basquin approximation relationship.

2. MATERIALS AND METHODS

2.1 Magnesium AZ31B

Magnesium Mg AZ31B was purchased commercially from Luoyang Maige Magnesium Industry Co., Ltd., China. The chemical composition of this material is shown in table 1. All samples have been cold-formed through an extrusion process based on the ASTM B107/B107M standard. Generally, the extrusion process is carried out below the metal's recrystallization temperature or at room temperature [19]. This extruded specimen has a diameter and length of 16 mm and 130 mm, respectively. Then magnesium is formed with a CNC machine, appropriate to the shape and size of the specimen in Figure 1, with cooling in the form of flowing water. Surface roughness is made up to <0.4, which is done to fulfill the fatigue test requirements.

The magnesium specimen is to be tested for the tensile property and then given in a symbol of Mg1T – Mg4T. The tensile test specimen was prepared based on the ASTM B557-02a standard (figure 1a). The fatigue-tested specimen was given the symbol of Mg3 – Mg12 and then tested based on ASTM E606-92 standard, as shown in figure 1b. The complete schema of the testing fatigue test is presented in Figure 2.

Table 1. Chemical composition of Mg AZ31B (wt.%)

Mg	Al	Zn	Mn	Fe
96,1	2,71	0,69	0,32	0,002
Si	Sn	Cu	Ni	Ca
0,18	<0,001	<0,001	<0,002	<0,001

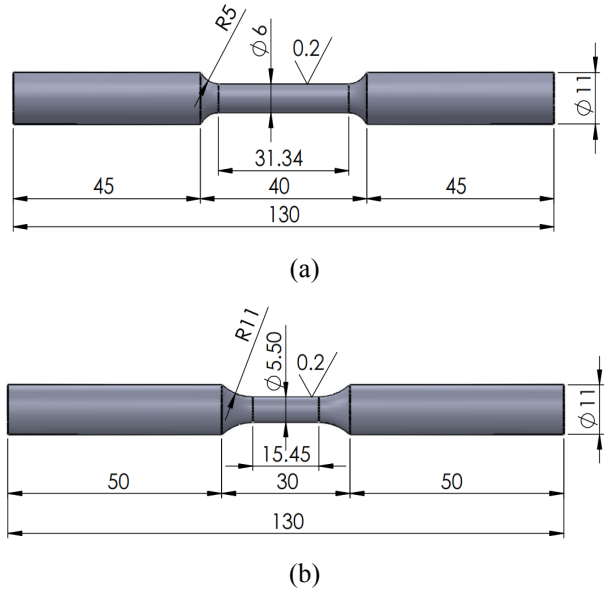

Figure 1. Specimen shape and size for (a) tensile test and (b) low cycle fatigue test (unit in mm)

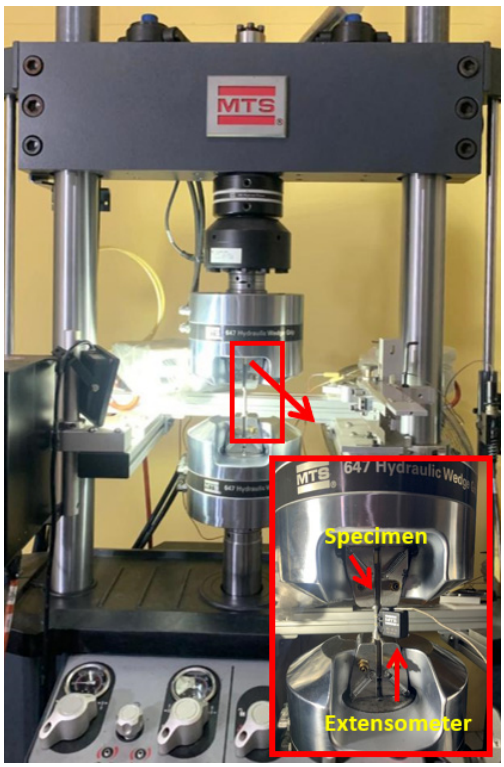

Figure 2. Detailed view of the experimental setup and mounting extensometer on the specimen.

2.2 Tensile and LCF tests

The low cycle fatigue and static tensile tests were carried out using servo-hydraulic computerized MTS Landmark 100 kN with Multipurpose Elite (MPE) soft–ware program for running the tests. Furthermore, the Mg specimens were tested under axial load to obtain their mechanical properties. The extensometers used were the MTS Axial Extensometers 10 mm (model 632.13F-20) installed at the gauge length area of the specimen. For the tensile test, the specimen was pulled axially at a constant speed of 0.15 mm/minute and 0.30 mm/minute until it broke. The difference in the pulling speed of the tensile test is used as a comparison to see the difference in the results after the tensile test. The stress-strain data obtained from extensometer measure–ments were plotted in the form of a curve. The modulus value of elasticity of Mg AZ31B was obtained using the least-squares method with a linear length range of the stress-strain curve of 20%. Furthermore, the 0.2% offset method was used to get the yield strength value.

Fifteen specimens for the LCF test were performed under an amplitude strain control of 0.004 – 0.01 mm/mm with a strain ratio (R) of -1 in sinusoidal wave at a constant strain rate of 0.00627 mm/mm/seconds. Furthermore, A different frequencies were calculated based on relation of strain amplitude and strain rate [20] which those frequency value for 0.004 mm/mm, 0.005 mm/mm, 0.006 mm/mm, 0.008 mm/mm and 0.01 mm/mm were 0.3919 Hz, 0.3135 Hz, 0.2613 Hz, 0.1599 Hz and 0.1568 Hz, respectively. LCF data, including plastic strain, elastic strain, stress amplitude, and elastic modulus, were determined at a half cycle (0.5Nf). The plastic and elastic strains data with reversals to failure cycles (2Nf) at all tested strain amplitudes were plotted

into a curve to predict service life using the Coffin-Manson-Basquin equation. The microstructure of Mg AZ31B for the behavior of plastic deformation or cyclic loading was observed using a Carl Zeiss Trinocular Metallurgical Microscope Type Axio Vert A1 Mat with an etching solution of HNO3 and alcohol.

3. RESULTS AND DISCUSSION

3.1 Microstructural observation

Dynamic loads tend to match with the application of bone bolts which sometimes experience repeated tensile or compressive loads. Therefore, magnesium alloys used as biomaterial must pass the fatigue testing first. The observed microstructure of Mg AZ31B is shown in Figure 3. Several methods generally carry out magnesium production, namely rolling, casting, and extrusion. The extrusion process changed the microstructure of Mg AZ31B, as shown in Figure 3.

Furthermore, the grains had an elongated and flat shape. The black spots (indicated by arrows) shown are aluminum which increases the hardness of magnesium, while the coarse and fine lines to are the deformation produced during the process of forming the metal due to tensile forces. This deformation is considerable at the surface area because the metal is being pulled, and the cross-section is fixed. Furthermore, the Mg AZ31B extrusion that has not been tested for fatigue shows an inhomogeneous grain size ranging from 5-10 µm.

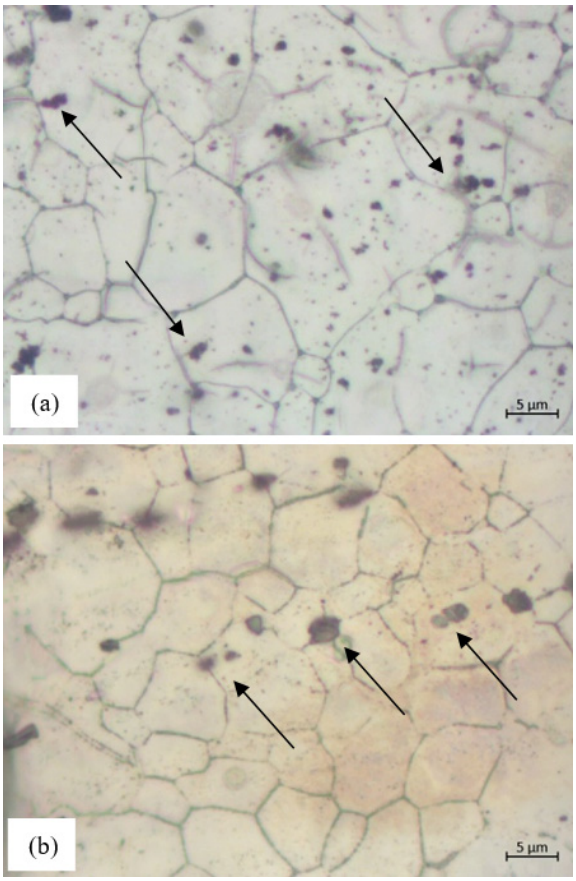

Figure 3. Original microstructure of Mg AZ31B in extrusion condition in (a) Transversal and (b) Longitudinal directions

Several small-sized grains are observed, and a small amount of the grains precipitated in the grain boundary zone. This shows that the recrystallization process occurs dynamically when the extrusion process is carried out. The metal formation process leads to large equiaxed grains. Also, the grain size of Figure 3b ranges from 5-15 µm, and the grain orientation direction follows a diagonal direction from bottom to top.

3.2 Hardness measurement

The indentation results of Mg AZ31B are shown in Figure 4. The hardness value decreases in the transverse section, closer to the midpoint or the center point. The value at the center point is only around 59.32 HV, while a further indentation point from the center has a value that increases to 63.13 HV and 63.99 HV. That was because the deformation at the central point area is smaller than the surface and the outer areas. The extrusion process will lead to higher deformation in the outer area.

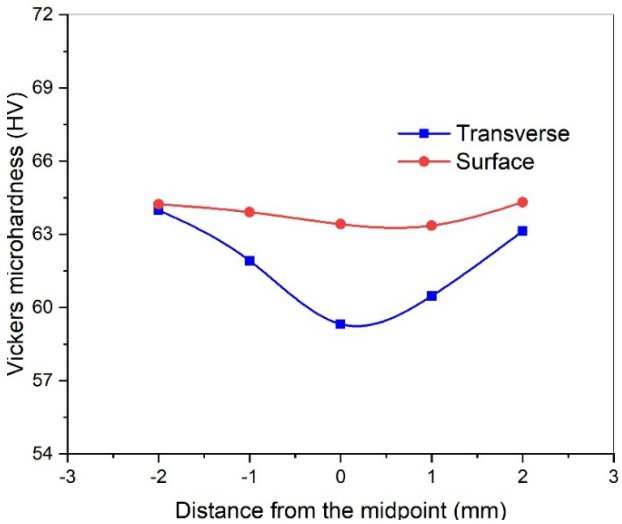

Figure 4. The profile of hardness values of extruded Mg AZ31B at different area

The modulus value of elasticity of Mg AZ31B was obtained using the least-squares method with a linear length range of the stress-strain curve of 20%. Fur–thermore, the 0.2% offset method was used to get the yield strength value. The tensile test results are shown in Table 2.

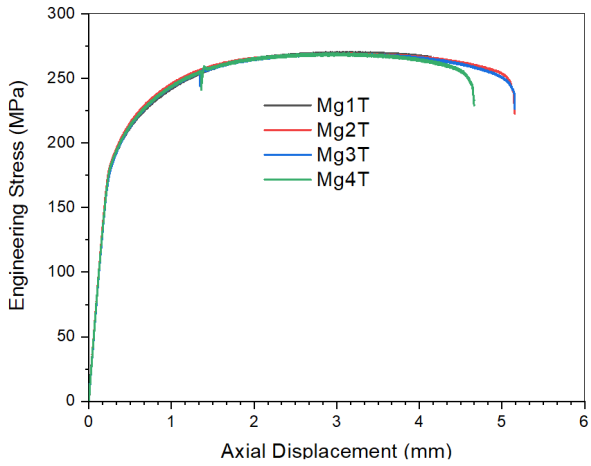

Figure 5. The relationship between the stress incremental and the change in specimen length

Table 2. Tensile test results

Specimen Name	Stress (MPa)		Plastic Energy (kJ)	Elastic Energy (kJ)	Reduction of Cross-sectional Area (%)	Total Elongation (%)
	Yield (0,2%)	Ultimate				
Mg1T*	185,15	270,45	0,0130	0,0070	Loss data	Loss data
Mg2T*	188,44	269,29	0,0120	0,0080	25,38	16,44
Mg3T*	184,45	269,13	0,0133	0,0079	24,23	16,45
Mg4T**	186,44	269,51	0,0200	0,0140	30,71	18,95

**Speed rate of 0.15mm/min*
***speed 0.30mm/min*

Table 3. Low cycle fatigue test results of Mg AZ31B

Specimen	Strain amplitude (mm/mm)	Frequency (Hz)	Plastic Strain (mm/mm)	Elastic Strain (mm/mm)	Modulus of Elasticity (GPa)	Number of Fracture Cycles (Nf)
Mg3	0,004	0,3919	0,000169	0,003831	45,16	5112
Mg4	0,004	0,3919	0,000220	0,003781	45,20	4985
Mg5	0,005	0,3135	0,000450	0,004550	44,62	1846
Mg6	0,005	0,3135	0,000478	0,004522	44,17	1319
Mg7	0,006	0,2613	0,001085	0,004916	44,11	1020
Mg8	0,006	0,2613	0,001166	0,004834	36,76	895
Mg9	0,008	0,1959	0,002783	0,005218	45,59	506
Mg10	0,008	0,1959	0,002753	0,005248	45,68	473
Mg11	0,010	0,1568	0,004365	0,005636	44,90	515
Mg12	0,010	0,1568	0,004510	0,005490	44,80	312

The relationship between incremental stress and axial displacement value for three specimens of ext–ruded Mg AZ31B is represented by stress vs. axial displacement curves in Figure 5. The LCF test results are presented in Table 3, while the hardness profile of Mg AZ31B in different areas is shown in Figure 6.

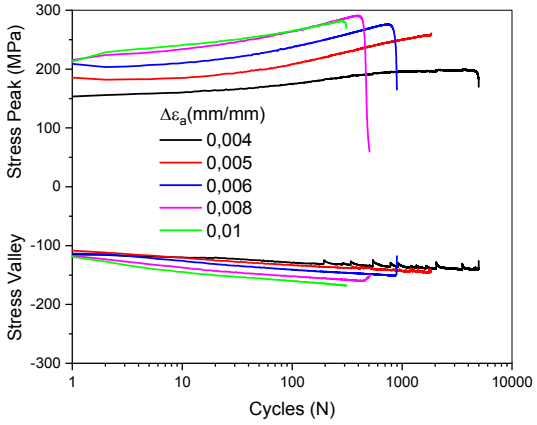

Figure 6. The profile of hardness values of extruded Mg AZ31B at different area

The effect of strain amplitude on fatigue cycles of extruded Mg AZ313B is represented by response ten–sions and compression stress, as shown in Figure 5. Also, the hardness profile of Mg AZ31B samples shows the hardened condition until the last cycle of the fatigue test, which will be discussed further in the following section.

3.3 Cyclic stress responses

Previously, research fatigue testing on bone bolts under cyclic conditions has been presented elsewhere [21]. High strain amplitude greatly affected the sample's life and their modulus of elasticity. Strain rate and frequency applied to bone bolts will affect their fatigue life. The depth of the bone bolt also plays an essential role in its fatigue. The longer the bone bolt, the higher the stiffness value of the bolt. Also, a study on the fatigue life of cortical bone bolts under cyclic conditions was conducted by others [22]. The results show that two critical factors affect fatigue life: the axial stress of the bolt (a normal force that occurs from plate to bone) and shear load due to cyclic loading [22].

The fracture occurs in the center of the bolt between the plate and the bone. The central region of the bolt is the initial initiation region for screw failure. The application of load applied to the bolt affects its fatigue life. The increasing of the applied load will shorten its fatigue life. Once the cyclic load was applied to a bone bolt below its yield strength, depending on the strain rate and its strain amplitude. The strain amplitude is increased, the fatigue fracture area is more prominent, and the fatigue life is much lower, as presented by others [23]. The pattern of failure and the shape of the fracture of each specimen test have a similar shape, so it can be concluded that cyclic loads cause the load received by the bolt during the testing process. The size of the bone bolts tested also affects the stability between the plate and the bone, although applying an accepted load can minimize this effect.

The results of the low cycle fatigue test in this study are shown in table 3, where the average value of the modulus of elasticity for Mg AZ31B was 44.35 GPa. Furthermore, the strain amplitude is inversely propor–tional to the number of fracture cycles produced. The value of the plastic strain compared to the elastic strain indicated a longer low cycle fatigue life. The modulus value of elasticity differed slightly from the static tensile and low cycle fatigue tests.

In Figure 6, the strain amplitude of 0.004 mm/mm showed that during the first cycle, the magnesium hardened until the last cycle. This continued until the specimen fractured. Furthermore, at a strain amplitude of 0.005 mm/mm, during the first cycle, magnesium softened until it reached the tenth cycle, then it hardened

until failures or fractures occurred. At a strain amplitude of 0.006 mm/mm, magnesium experienced a softening cycle from the first to third cycles. Mean–while, it hardened until it fractured from the fourth cycle. Furthermore, at a strain amplitude of 0.008 mm /mm, there was an increase in hardening from the first cycle to the last cycle. The failure or fracture that occurred in magnesium was in the plastic area.

The cyclic stress-strain response for cyclic hardening or softening depends on the dislocation substructure's stability. Generally, the dislocation density is initially low in soft materials such as Mg AZ31B. Due to cyclic plastic straining, the dislocation density will increase, becoming harder or stronger (cyclic hardening). Furthermore, cyclic plastic straining leads to dislocation stretching, reducing resistance to deformation (cyclic softening), as presented elsewhere [24]. Cyclic hardening or softening occurs only at the beginning of fatigue (± 20 – 40% fatigue life) and then stabilizes (± 50% fatigue life).

This test showed that the strain amplitude and the resulting cycle were in inverse proportion. For a strain amplitude of 0.01 mm/mm, the first to third cycles led to very high hardening. For the fourth cycle magnesium continued to harden until it fractured, making its hardening unlike the first to third cycles. Also, magnesium did not break or fail at an amplitude of 0.008 mm/mm, but when viewed closely, there was a crack initiation at the bottom of the cross-section. The two specimens tested at an amplitude of 0.008 mm/mm did not break or fracture and had only a few short cracks in the reduction section of the cross-section.

3.4 Cyclic stress-strain behavior

Figure 7 shows the Mg AZ31B hysteresis curve plot at different strain amplitudes.

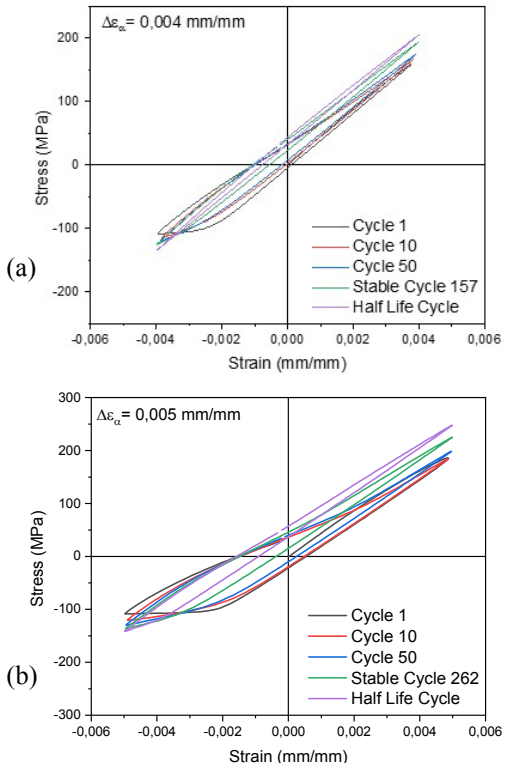

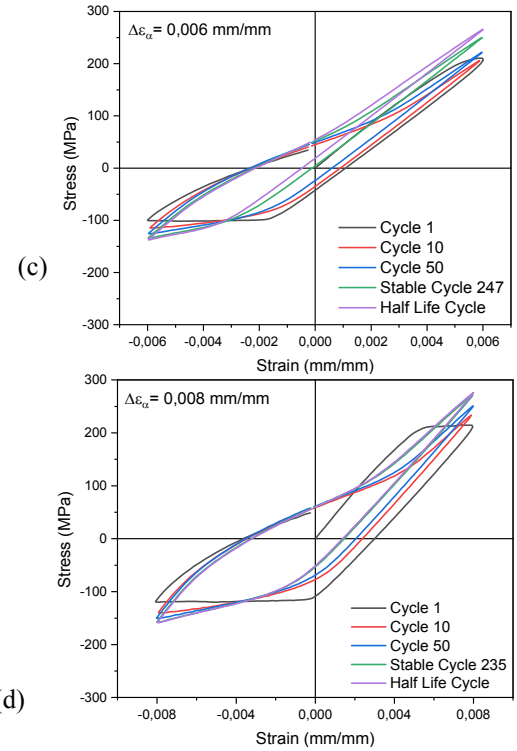

Figure 7. Hysteresis curve of the extruded Mg AZ31B at different fatigue cycles (in mm/mm) of (a) 0.004, (b) 0.005, (c) 0.006, (d) 0.008, and (e) 0.01

The evolution of the hysteresis curve in Figure 7a shows that magnesium undergoes cyclic hardening and a slight increase in compressive stress. This means that magnesium responds and undergoes some work hardening. There was also a gradual increase until stable cyclic hardening was observed from 157 cycles until magnesium failed. Furthermore, at a higher strain amplitude of 0.005 mm/mm (Figure 7b), the behavior of magnesium undergoes progressive cyclic softening with decreasing peak stress and increasing number of cycles.

Cyclic softening occurs due to a reduction in dis–location densities and an inhomogeneous arrangement of dislocations, which leads to several empty spaces. There–fore, when loading is carried out, there will be a prog–ressive cyclic softening during the initial to tenth cycles. Figures 7c to 7e show the effect of the extrusion process, which significantly changes the magnesium behavior du–ring the deformation process. Furthermore, during the first to third cycles, the magnesium undergoes softening fol–lowed by cyclic hardening until failure. The micro–struc–ture of the tested specimen at the strain amplitude of 0.006 mm/mm using an optical microscope is shown in Figure 8.

The grain boundaries appear more pronounced with a size of 5-15 µm-the method of calculating the size with the expansion of the area contained in the system application. Several parallel lines are evenly distributed over most of the grains. The grain size originates from deformation due to the formation process or dislocation. In Figure 8a, it ranges from 5-15 m, and the orientation direction looks like a diagonal from bottom to top. After carrying out the fatigue test, as shown in Figure 8b, there were parallel lines due to a large enough deformation, called twinning (represented with arrows). The orientation direction was the same as before the fatigue test, with a grain size of 5-40 m.

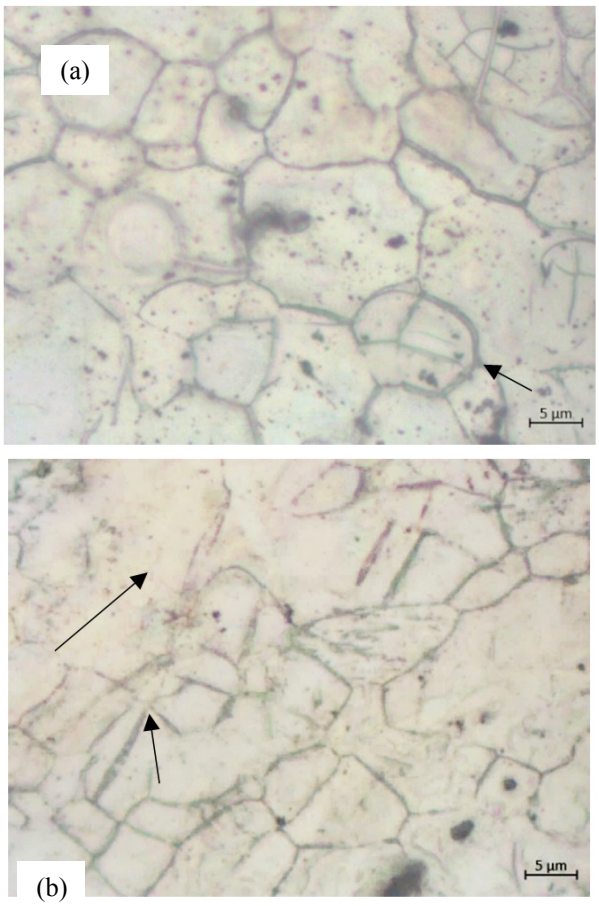

Figure 8. Change of microstructural observation on (a) Transverse surface section (b) Longitudinal surface section in LCF condition at a stress amplitude of 0.006 mm/mm

These lines exist due to the cyclic load applied to the sample. Therefore, the deformation caused by the load changes the grain size and shape. Furthermore, stress concentration is caused by grain boundaries and dislocations, both of which lead to crack initiation. The shape and orientation of the grains change with the crack propagation direction to follow a new groove or when the crack propagation encounters a complicated composition grain such as aluminum.

After fatigue testing, not all grains have perfect shapes, and several tend to be flat, elongated, and very large, with obvious boundaries along the cross-section in the microscope. The deformation in magnesium is closely related to cyclic softening and hardening, which can be calculated using equations (1) and (2). The cyclic softening of the Mg AZ31B in a low cycle test with a constant strain rate of 0,00627 is presented in Figure 9.

Cycle softening ratio:

$$S = 1 - \frac{\left(\sigma_{peak}\right)Nf/2}{\left(\sigma_{peak}\right)N=1} \tag{1}$$

Cycle hardening ratio:

$$H = \frac{\left(\sigma_{peak}\right)Nf/2}{\left(\sigma_{peak}\right)N=1} - 1 \tag{2}$$

Based on the results and discussion of the experiment, it can be concluded that dislocation slip and twinning occur during fatigue deformation. During the test process, strain hardening characteristics can be found throughout the fatigue process. Each cycle increases, the macroscopic plastic strain amplitude decreases, and the stress amplitude increases. The cyclic hardening in this test can be attributed to an increase in dislocation density, the material's response during the test process, and the interaction of dislocations with precipitates during plastic deformation. The study [24] observed the cyclic deformation behavior of Mg AZ31B with a low cycle fatigue test. Cyclic hardening can be observed at higher total strain amplitudes.

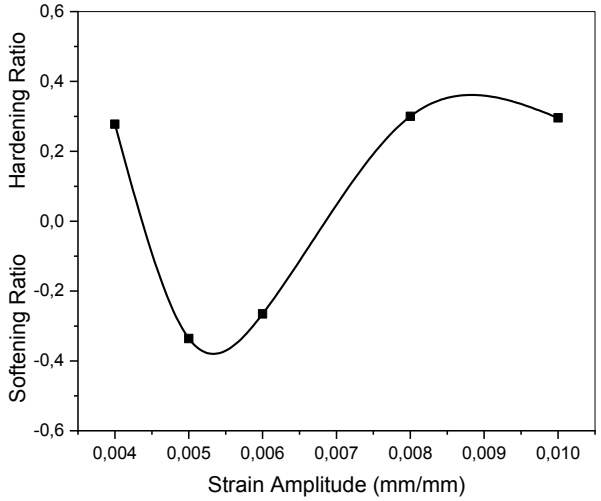

Figure 9. The cyclic softening or hardening ratio of magne–sium in the LCF test with a constant strain rate of 0.00627 1/seconds.

The results showed that cyclic hardening could be observed during the fatigue test process. At lower strain amplitudes of the Mg AZ31 test, the cyclic stress amp–litude remains essentially constant compared to the static tensile test resulting in higher cyclic hardening, known as fatigue failure cyclic hardening mechanism [25]. Cross-slipping and twinning dislocations are the leading causes of the cyclic hardening process. The formation and increase of dislocations cause the har–dening during the test process, and magnesium responds so that interactions occur and form twinning. One of the twins' contributions is to develop a pseudoelastic behavior at given stress above its capacity [25,26].

In addition, twins cause cyclic hardening due to dislocation shifts. Hardening can arise from the conf–luence of several dislocations and the inhibition of dislocation movement caused by the twinning boundary. Primary cyclic hardening occurs only when the fatigue limit is exceeded, as indicated by the rapid increase in hardening, which is constant as the maximum stress increases. Other results also show that prismatic slip becomes active beyond its fatigue limit and is involved in the cyclic hardening process.

Magnesium undergoes a transition from cyclic softening to hardening when the strain amplitudes of 0.006 and 0.008 mm/mm are the saturation points. The dislocation slips and twinning phenomena occurred during fatigue deformation. During the test process, strain hardening characteristics were discovered throughout the fatigue process. Also, as each cycle increases, the macroscopic plastic strain amplitude

decreases, and the stress amplitude increases. The cyclic hardening can be attributed to an increase in dislocation density, the material response during the test process, and the interaction of dislocations with precipitation during plastic deformation.

Magnesium, especially the AZ31B type, has a unique feature: the Bauschinger effect. This effect often occurs when the material is soft and tends to brittle, the graphic looks not like a symmetrical leaf but tends to be broad, and this effect can be seen when the material is compressed. [26] observed phenomena, which in this study used their suggestions as estimates that fit within the criteria for yield strength under compressive stress. Different parameters have been used to measure the Bauschinger effect. The Bauschinger Effect Factor is the ratio between the yield strength after a reversal load (in compression or compression stress) and the maximum tensile stress proposed by others [26]. The Bauschinger strain, described as the strain used (after load reversal), may affect stress equal to the maximum tensile stress before unloading, as presented in Figure 10 [26].

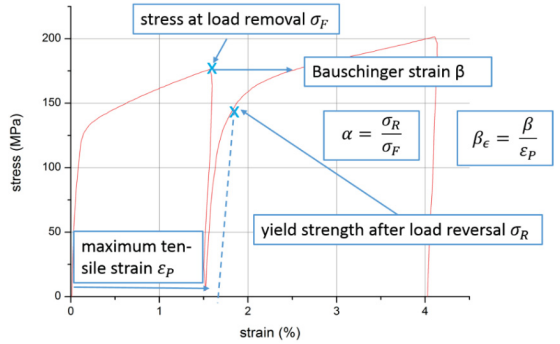

Figure 10. Stress-strain curve of compressive stress [26]

The data of this study's Bauschinger effect factor (BEF) was calculated and presented in table 4. Once the BEF value is 1.0, it means that there is no Bauschinger effect occurred on the tested material.

Table 4. Bauschinger effect factor calculation result

Strain Amplitude (mm/mm)	σ_f	σ_R	β	ε_p	α	β_ε
0,006	114,45	112,60	0,00612	0,00726	0,98379	0,84344
0,008	117,28	113,53	0,00804	0,01096	0,96799	0,73289
0,010	118,94	112,59	0,01000	0,01470	0,94667	0,68023

The BEF value decreases slightly with increasing maximum tensile strain, as for a strain amplitude of 0.006, it is 0.98, for a strain amplitude of 0.008, it is 0.96, and for a strain amplitude of 0.01, it is 0.94. On the other hand, the Bauschinger strain decreases with increasing tensile strain: for a strain amplitude of 0.006, it is 0.84, the strain amplitude of 0.008 is 0.73, and for a strain amplitude of 0.01, it is 0.68. This result is similar to an austenitic stainless steel AISI 304 material that has been presented elsewhere [27]. The Bauschinger effect occurs quite large after 20% strain, and kinematic hardening occurs when 1/3 of the yield strength. A strain>3% of the reverse stress change shows a real linear line and permanent softening.

Hardening behavior occurs due to a combination of isotropic hardening and kinematic hardening. The result of the average yield strength is being used as a parameter, and a more considerable offset value will result in higher isotropic hardening. Other research has concluded that the Bauschinger effect (BE) was observed on magnesium AZ31 tested with compression and cyclical tension mechanisms [28]. It was shown that the Bauschinger effect is seen during pre-strain compression. Observations of the microstructure and grain orientation during stress and compression cycles indicate that the cause of the Bauschinger effect is a combination of re-orientation in pre-compression and detwinning effects formed during the compression cycle, which causes the yield strength to decrease [28].

Although the grain orientation does not change, a decrease in the c/a ratio will restrain the rate of twinning formation during the re-compression process. Similar to other results, the Bauschinger effect was also observed on the austenitic stainless steel Mn18Cr18N [29]. In the smaller cyclic strain amplitudes, the intergranular back stress is the primary source of the Bauschinger effect. With increasing cycles, the dislocation density increases, and the dislocation movement rate is inhibited when deformation occurs.

The Bauschinger effect weakens to some extent, while at higher cyclic strain amplitudes, the reverse stress originating from dislocation piles at the grain boundaries and twinning formation due to continuous deformation [29]. Further calculation of the plastic strain amplitude of Mg AZ31B is presented in Fig. 11.

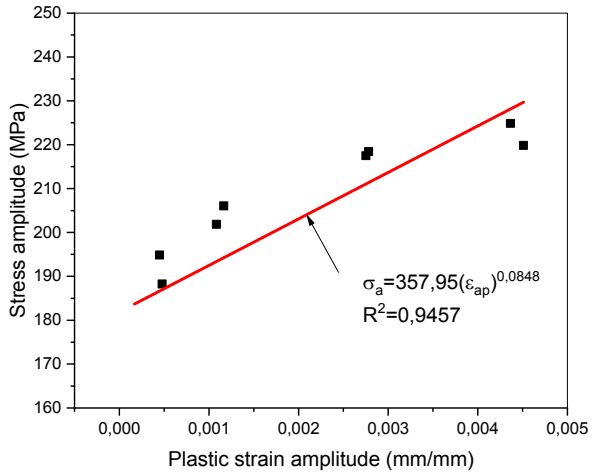

Figure 11. The plastic strain amplitude vs. stress amplitude curve

Based on Figure 11, the coefficient of cyclic stren–gth, K', and the cyclic strain-hardening exponent, n', are obtained from the stress-strain plot of magnesium in the plastic region. K' and n' are shown in table 5.

Table 5. Low cycle fatigue properties of Mg AZ31B

LCF parameters	Value
Coefficient of cyclic strength, K' (MPa)	357,95
Fatigue strength coefficient, σ'_f (MPa)	534,17
Cyclic strain-hardening exponent, n'	0,0848
Fatigue strength exponent, b	-0,1463
Fatigue ductility coefficient, ε'_f (mm/mm)	8,12
Fatigue ductility exponent, c	-1,2827

Using that result, a graphic of the relation of strain amplitude against the number of failure cycles (2Nf) can be plotted, as shown in Figure 12.

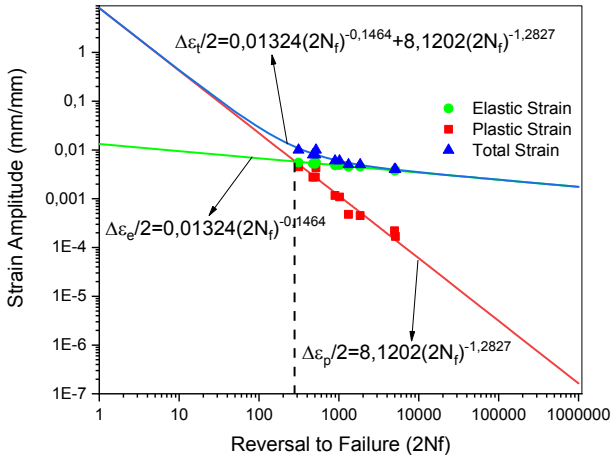

Figure 12. Strain amplitude curve vs. number of reciprocal fracture cycles (2Nf)

3.5 Fractographical observation

Strain amplitude of 0.006 mm/mm, which has been tested by LCF, fractographic observations were made using SEM. Figure 13 shows some pictures that have been taken at 40x, 500x, and 2000x magnification. Cracks due to fatigue testing basically start from the surface of the specimen. At the micro magnification level, magnesium's fracture process generally begins with microvoids' growth or cracks in the first phase; after that, local failure occurs in the second phase of the particles such as precipitates, oxides, or inclusions or intermetallic particles.

Figure 13 shows the typical SEM test results for fracture morphology of the Mg 8 specimen tested for fatigue at a strain velocity of 0.00627 1/s and a strain amplitude of 0.006 mm/mm. If observed with low magnification on the fracture surface, there are cleavage surfaces in some of the fracture areas. Cleavage surfaces occur in materials with a relatively large grain structure and tend to fracture at low temperatures.

In the crack initiation region, there is an elongated cleavage. This can be attributed to the material's coarse and large grain size as it approaches the surface. The (a) iform grain size distribution and the much larger grain near the surface lead to early cracking. Catastrophic failure is caused by materials that tend to break brittle and, in many cases, occur due to fatigue testing. However, many also occur due to fatigue. While fatigue testing takes place, crack growth occurs from time to time during the testing process. Figures 13(a) to 12(c) show the direction of fatigue crack propagation from the right side to the left until the catastrophic failure; the fatigue area looks like a dotted line. This catastrophic failure phenomenon is observed after the final failure when the critical crack length is reached.

The appearance of a cleavage surface or a river-like pattern is formed when crack propagation in the grain boundary region has occurred at different orientations and through a gradual process. These cleavage surface grooves tend to coalesce in the direction of crack growth, and they can be used to identify local crack initiation and growth events. Many small areas with river-like patterns can be seen in Figures 13(d) to 13(f).

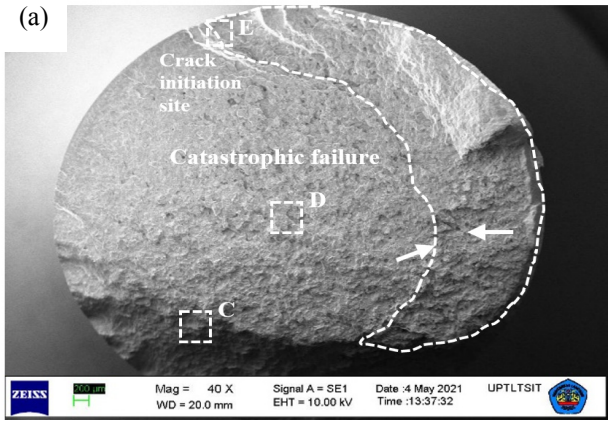

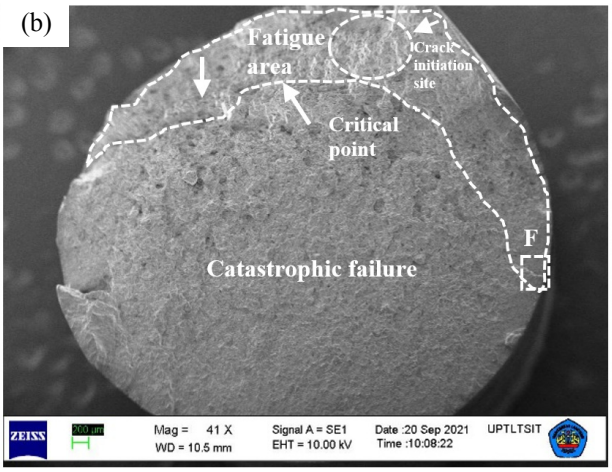

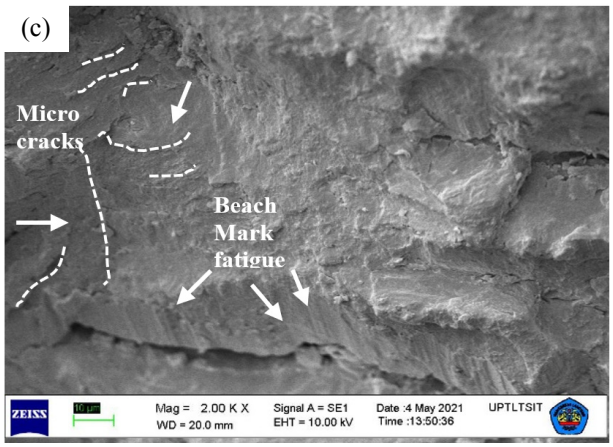

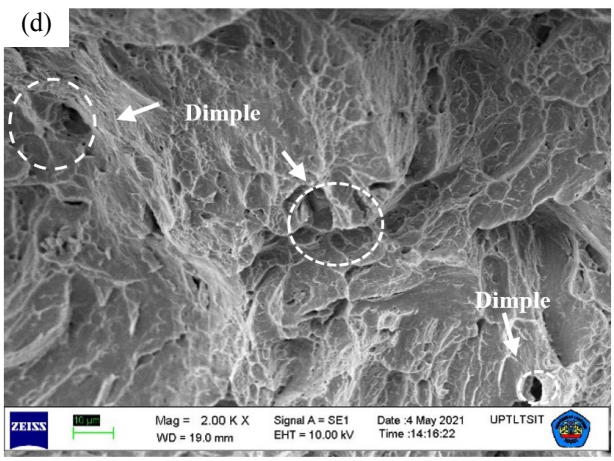

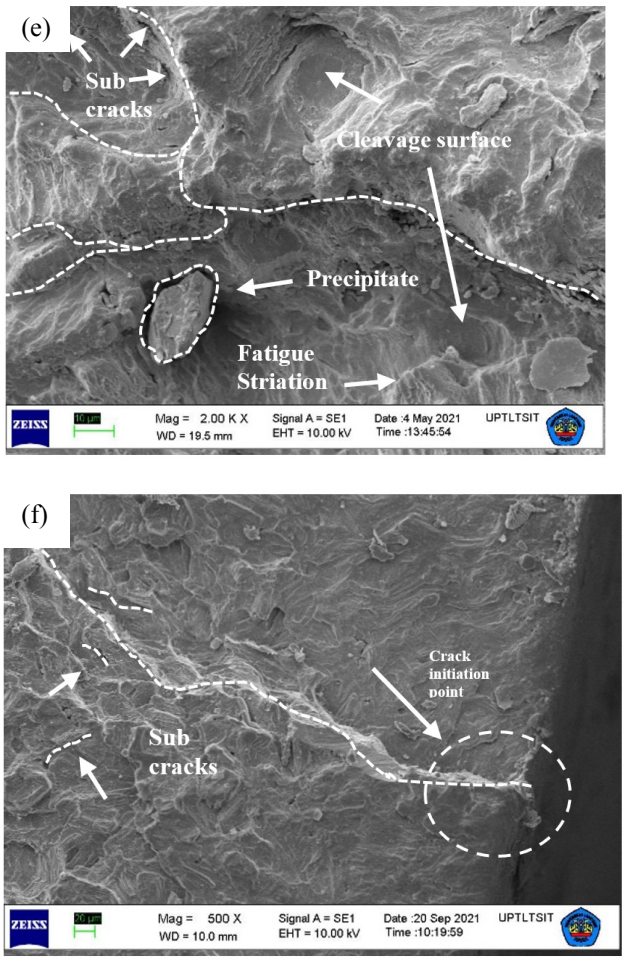

Figure 12. SEM of the fracture surface on LCF samples with a strain amplitude of 0.006 mm/mm

Further analysis of the fracture surface, as on figure 13(a), it consists mostly of cleavage or brittle intergranular facets; there is a crack resembling a river pattern that propagates from the crack initiation; after that, on the lower right side, there is a small amount of fatigue striation and in the plastic deformation zone. Also, more dimples are found, as shown in figure 13(d), due to a typical catastrophic failure which refers to static fracture after crack propagation reaches the critical area and then fractures.

A static fracture occurs after the critical crack length is formed until it is unable or no longer able to withstand the given cyclic load. As indicated by the arrows in figure 13(a), many second-phase particles were also observed at the fracture surface. It could be either the origin of the fracture or the fracture initiation region. Micro cracks are also shown in figure 13(c), with some beach marks of fatigue. The shoreline marks point perpendicular to the tensile stress, which are signs of crack propagation. After spreading such that the remaining cross-section can no longer withstand the working load, a final fracture or static fracture occurs. The area between the crack propagation stage and the final fracture stage can quantitatively indicate the magnitude of the working stress. If the area of the crack propagation stage is greater than the area of the final fracture area, then the working stress is relatively low, and vice versa. Beach mark fatigue occurs due to fatigue in the material that propagates in a radial direction. It is a characteristic or sign of crack propagation that occurs when there is more than one crack initiation location.

A large number of dimples can be observed on the fracture surface, which indicates that the material in this area undergoes considerable plastic deformation at a strain rate of 0.00627 1/s and a strain amplitude of 0.006 mm/mm, as in figure 13(d). There was a close relati–onship between the constituent matrix and the second phase of the particles. The movement of dislocations during the low cycle fatigue test and the number of dislocations at grain boundaries significantly affect the formation of dimples. However, in mixed magnesium, for example, Mg AZ31B, it can cause nucleation of micro-voids in the center of the magnesium sample. Then, the small micro-voids coalesce to form larger voids. The presence of voids in the center of the sample will trigger magnesium failure caused by the unstable pressure that exists when the core area of the sample can no longer support the given load. As a result, the magnesium sample will fail and fracture on the surface due to shear forces which will form dimples.

Based on the fatigue data, microstructure, fracto–graphy displayed, and the AZ31B Mg capability, this material is very suitable for implants. Other materials such as 316L SS, Co-Cr alloys, and titanium have significant weaknesses, such as poor corrosion and wear resistance, can cause allergies easily, toxic when CoCrNi ions are released, and their fatigue properties are different from human bone. The condition of the human body also demands an implant material that tends to be lightweight but has strength and can with–stand high cycle loads. This process occurs when implantation causes wear and tear, triggering a material layer reaction [30, 31].

The morphology of biomaterial must be easily acceptable by the body. This is incompatible with human bone morphology, but the concept will differ if applied to joints. Fatigue testing methods for bioma–terials should include tests of morphological charac–teristics to simulate conditioned stress-strain in vivo. Another example was developed on titanium, which has been fatigue tested for a long time; fatigue testing can take up to high cycles. It is still a challenge for engineers to find biomaterials that are easy to obtain and accept by the body [31,32].

4. CONCLUSION

The yield stress value is taken from the average specimen value for fatigue testing, y = 186.01 MPa, and the elastic modulus (E) = 43.72 GPa. The low strain amplitude will extend the life according to the number of fracture cycles. The behavior of magnesium undergoes a strain hardening cycle and a strain-softening cycle during a low cycle fatigue test with different strain amplitude variations. Cyclic softening of Mg AZ31B occurred at strain amplitudes of 0.005 and 0.006 mm/mm, and cyclic hardening at strain ampli–tudes of 0.008 and 0.01 mm/mm, while cyclic strain hardening founded at higher amplitude parameters. The Bauschinger effect was observed at strain amplitudes above 0.6%, leading to a significant difference between the tensile and compressive yield stresses, and the

hysteresis loop becomes asymmetrical. The twinning-de-twinning defects occur during the compression process and continue until fracture. Fatigue life increases with decreasing strain amplitude that, evaluated using the Coffin-Manson-Basquin equation, shows a potential application of AZ31B for bone bold and other biomedical material.

REFERENCES

[1] Castro, F., & Jiang, Y. Fatigue of extruded AZ31B magnesium alloy under stress-and strain-controlled conditions including step loading. Mechanics of Materials, 108, 77-86. 2017.

[2] Buldum, B. B., Aydın, S. I. K., & Ozkul, I. Investigation of magnesium alloys machinability. International Journal of Electronics Mechanical and Mechatronics Engineering, 2(3), 261-268. 2013.

[3] Rajan, A. V., Sundaram, C. M., & Rajesh, A. V. Mechanical and morphological investigation of bio-degradable magnesium AZ31 alloy for an orthopedic application. Materials Today: Proceedings, 21, 272-277. 2020.

[4] Prakash, C., Singh, S., & Ramakrishna, S. Characterization of indigenously coated biode–gradable magnesium alloy primed through novel additive manufacturing assisted investment casting. Materials Letters, 275, 128-137. 2020.

[5] Hart, N. H., Nimphius, S., Rantalainen, T., Ireland, A., Siafarikas, A., & Newton, R. U. Mechanical basis of bone strength: influence of bone material, bone structure and muscle action. Journal of musculoskeletal & neuronal interactions, 17(3), 114. 2017.

[6] Rodrigues, A., Caetano-Lopes, J., Nery, A., Sousa, E., PoIido-Pereira, J., VaIe, M., & Canhão, H. Evaluation of Bone Mechanical Strenght and Fracture Risk Assessment [Frax] In Patients with Hip Joint Replacement Surgery. Acta reumatologica portuguesa, 34(3). 2009.

[7] Radha, R., & Sreekanth, D. 2017. Insight of magnesium alloys and composites for orthopedic implant applications–a review. Journal of magnesium and alloys, 5(3), 286-312.

[8] Chen, G., Gao, J., Cui, Y., Gao, H., Guo, X., & Wu, S. Effects of strain rate on the low cycle fatigue behavior of AZ31B magnesium alloy processed by SMAT. Journal of Alloys and Compounds, 735, 536-546. 2018.

[9] Hasegawa, S., Tsuchida, Y., Yano, H., & Matsui, M. Evaluation of low cycle fatigue life in AZ31 magnesium alloy. International Journal of Fatigue, 29(9-11), 1839-1845. 2007.

[10] Faruk, M. E. R. T. Wear behaviour of hot rolled AZ31B magnesium alloy as candidate for biodegradable implant material. Transactions of Nonferrous Metals Society of China, 27(12), 2598-2606. 2017.

[11] Zhang, L. C., Xu, M., Hu, Y. D., Gao, F., Gong, T., Liu, T. & Pan, C. J. Biofunctionization of biodegradable magnesium alloy to improve the in vitro corrosion resistance and biocompatibility. Applied Surface Science, 451, 20-31. 2018.

[12] Šljivić, M., Stanojević, M., Djurdjevic, D., Gru–jovic, N. and Pavlović. Implemenation of FEM and rapid prototyping in maxillofacial surgery. FME Transactions, 44(4), 422-429. 2016.

[13] Chowdhury, S. M., Chen, D. L., Bhole, S. D., Cao, X., Powidajko, E., Weckman, D. C., & Zhou, Y. Tensile properties and strain-hardening behavior of double-sided arc welded and friction stir welded AZ31B magnesium alloy. Materials Science and Engineering: A, 527(12), 2951-2961.

[14] Witte, F., Hort, N., Vogt, C., Cohen, S., Kainer, K. U., Willumeit, R., & Feyerabend, F. 2008. Degradable biomaterials based on magnesium corrosion. Current opinion in solid state and materials science, 12(5-6), 63-72. 2010.

[15] Witte, F., Kaese, V., Haferkamp, H., Switzer, E., Meyer-Lindenberg, A., Wirth, C. J., & Windhagen, H. In vivo corrosion of four magnesium alloys and the associated bone response. Biomaterials, 26(17), 3557-3563. 2005.

[16] Sezer, N., Evis, Z., Kayhan, S. M., Tahmasebifar, A., & Koç, M. Review of magnesium-based biomaterials and their applications. Journal of magnesium and alloys, 6(1), 23-43. 2018.

[17] Jabbari, A. H., Sedighi, M., Jahed, H., & Sommitsch, C. Low cycle fatigue behavior of AZ31B extrusion at elevated temperatures. Inter–national Journal of Fatigue, 139, 105803. 2020.

[18] Morita, S., Ohno, N., Tamai, F., & Kawakami, Y. Fatigue properties of rolled AZ31B magnesium alloy plate. Transactions of Nonferrous Metals Society of China, 20, s523-s526. 2010.

[19] Thangaiah, S.I., Sevvel, P., Satheesh, C. and Jaiganesh, V. Investigation on the impingement of parameters of FSW process on the microstructural evolution & mechanical properties of AZ80A Mg alloy joints. FME Transactions, 46(1), 23-32. 2018.

[20] Badaruddin, M., Wardono, H., Wang, C.J., Rivai, A.K., Improvement of low-cycle fatigue resistance in AISI 4140 steel by annealing treat–ment. Inter–national Journal of Fatigue, 125, pp.406-417. 2019.

[21] Wu, Z., Nassar, S. A., & Yang, X. Axial fatigue performance of medical screws in synthetic bone. International Journal of Biomedical Engineering and Technology, 17(2), 192-207. 2015.

[22] Zand, M. S., Goldstein, S. A., & Matthews, L. S. Fatigue failure of cortical bone screws. Journal of biomechanics, 16(5), 305-311. 1983.

[23] Baumann, *M. Screw Pull Out under Cyclic Fatigue Loading in Synthetic and Cadaveric Bone* (Doctoral dissertation, The Ohio State University). 2015.

[24] Begum, S., Chen, D. L., Xu, S., & Luo, A. A. Low cycle fatigue properties of an extruded AZ31 magnesium alloy. International Journal of Fatigue, 31(4), 726-735. 2009.

[25] Szata, M., Lesiuk, G. A new method of constructing the kinetic fatigue fracture diagrams:

Crack propagation equation based on energy approach. FME Transactions, 36(2), 75-80. 2008.

[26] Härtel, M., Illgen, C., & Wagner, M. F. Experimental evaluation of Bauschinger effects during tension-compression in-plane deformation of sheet materials. In IOP Conference Series: Materials Science and Engineering (Vol. 118, No. 1, p. 012018). IOP Publishing. 2016.

[27] Manninen, T., Myllykoski, P., Taulavuori, T., & Korhonen, A. S. Large-strain Bauschinger effect in austenitic SS sheet. Materials Science and Engineering: A, 499(1-2), 333-336. 2009.

[28] Guangmin, S., Gongting, Z., Chun, Y., Research of bauschinger effect of AZ31 magnesium alloy. Rare Metal Materials and Engineering, 40(4), pp. 615-619. 2011.

[29] Li, F., Zhao, X., Zhang, H., He, W., Chen, H., & Guo, H. Bauschinger Effect of Mn18Cr18N Aus–tenitic Stainless Steel. Journal of Wuhan University of Technology-Mater. Sci. Ed., 35, 399-406. 2020.

[30] Teoh, S.H., 2000. Fatigue of biomaterials: a review. International journal of fatigue, 22(10), pp.825-837. 2000.

[31] Ibrahim, F. and Sukmana, I., 2021. Application of magnesium alloys in orthopedic implant. Jurnal Polimesin, 19(2), pp.182-187.

[32] Leitner, M., Stoschka, M., Schanner, R. and Eichlseder, W. Influence of high frequency peening on fatigue of high-strength steels. FME transactions, 40(3), 99-104. 2012.

ОСОБИНЕ НИСКОЦИКЛИЧНОГ ЗАМОРА ЕКСТРУДИРАНОГ МАГНЕЗИЈУМА АЗ31Б

И. Сухмана, Ф. Ибрахим, М: Бадарудин, Х. Нур

Понашање магнезијума (Мг) АЗ31Б при нискоцикличном замору је посматрано на собној температури, при чему је његов процес екструзије довео до разлика у затезним и притисним напонима, уз повећање структуре зрна и механичких својстава. Резултати процеса екструзије су показали промене у микроструктури услед цикличног оптерећења-де–формације на уздужном пресеку са смером и об–ликом зрна. Штавише, Мг АЗ31Б је такође показао прелазно понашање од цикличног омекшавања до очвршћавања када је амплитуда деформације пове–ћана. При амплитуди деформације од 0,006 – 0,01 мм/мм уочен је Баушингеров феномен. Фактор ефекта је израчунат на основу напона течења и деформације при напону компресије.

Штавише, падавине или локални квар друге фазе били су главни фактор који је изазвао Баушингеров феномен. Карактеристике лома услед замора засно–ване на деформацији услед цикличног оптерећења укључују падавине, заморне пруге, рупице, микро-пукотине и замор трагова на плажи. Стога је корелација укупног циклуса квара са пластиком и еластичном деформацијом добијена као једначина за предвиђање животног века Мг АЗ31Б.